Structure and Reactivity of II-VI and III-V Magic-Sized Clusters: Understanding and Expanding the Scope of Accessible Form and Function

Hunter H. Ripberger, Soren F. Sandeno, Forrest W. Eagle, Hao A. Nguyen, and Brandi M. Cossairt*

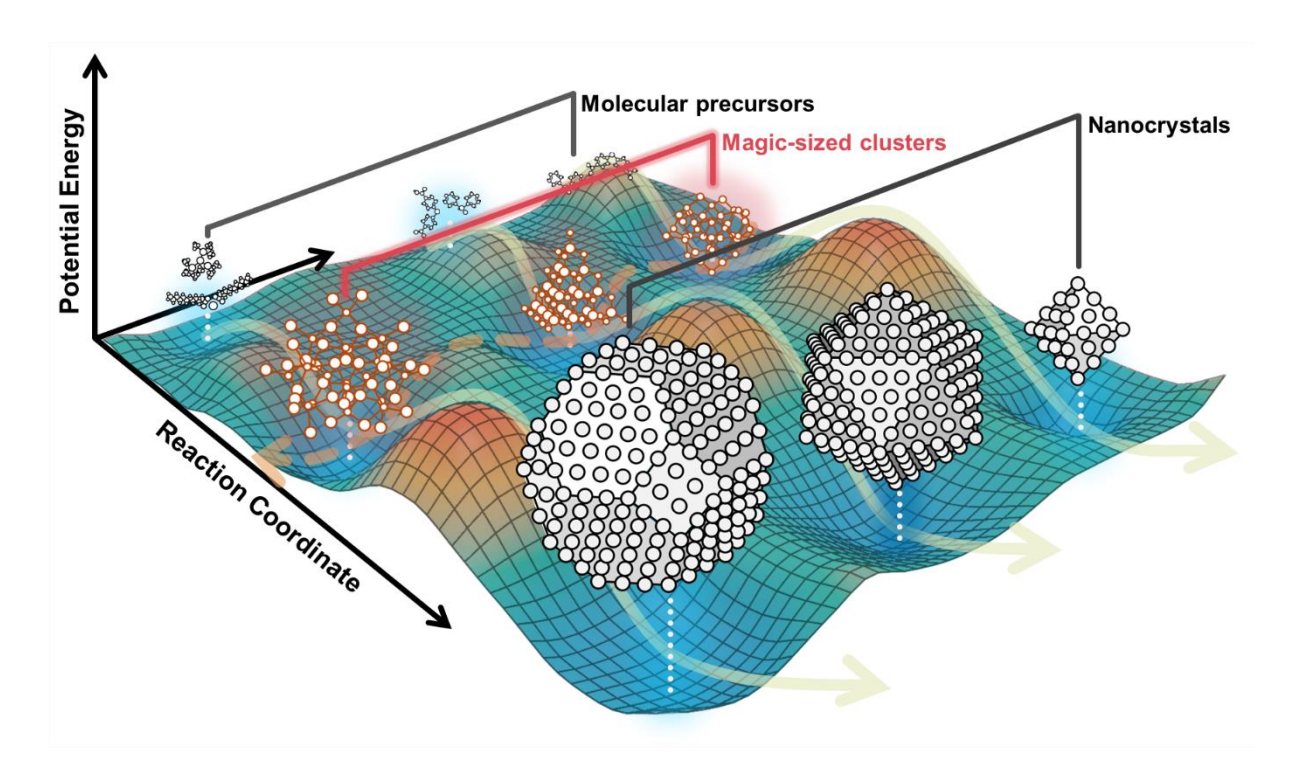
Department of Chemistry, University of Washington, Box 351700, Seattle, Washington 98195-1700, United States

*cossairt@uw.edu

Conspectus

In nanoscale chemistry, magic-sized clusters (MSCs) stand out for their precise atomic configurations and privileged stability, offering unprecedented insights into the atomic-level structure of ligand-capped nanocrystals and a gateway to new synthesis and functionality. This article explores our efforts to shed light on the structure and reactivity of II-VI and III-V semiconductor MSCs. We have specifically been interested in the synthesis, isolation, and characterization of MSCs implicated as key intermediates in the synthesis of semiconductor quantum dots. Our exploration into their synthesis, structure, transformation, and reactivity provides a roadmap to expand the scope of accessible semiconductor clusters with diverse structures and properties. It paves the way for tailor-made nanomaterials with unprecedented atomlevel control. In these studies, atomic level structure has been deduced through advanced characterization methods, including single-crystal and powder X-ray diffraction, complemented by pair distribution function analysis, nuclear magnetic resonance spectroscopy, and vibrational spectroscopy. We have identified two distinct families of CdSe MSCs with zincblende and wurtzite-like structures. We have also characterized two members of the wurtzite-like family of InP clusters and a related InAs cluster. Our research has revealed intriguing structural homologies between II-VI and III-V MSCs. These findings contribute to our fundamental understanding of semiconductor MSCs and hint at broader implications for phase control at the nanoscale and the synthesis of novel nanomaterials. We have also explored three distinct pathways of cluster reactivity, including cluster interconversion mediated by controlling the chemical potential of the reaction environment, both seeded and single source precursor growth mechanisms to convert MSCs into larger nanostructures, and cation exchange to access new cluster compositions that are precursors to nanocrystals that may be challenging or impossible to access from traditional bottomup nucleation and growth. Together with the collective efforts of other researchers in the field of semiconductor cluster chemistry, our work establishes a strong foundation for predicting and controlling the form and function of semiconductor MSCs. By highlighting the role of surface chemistry, stoichiometry, and dopant incorporation in determining cluster properties, our work opens exciting possibilities for the design and synthesis of new materials. The insights gained through these efforts could significantly impact the future of nanotechnology, particularly in areas like photonics, electronics, and catalysis.

Conspectus Graphic



Caption: Schematic diagram of molecular precursors, MSCs, and nanocrystals on a potential energy surface.

Introduction

In the field of chemistry at the nanoscale, a class of remarkable structures emerges: magic-sized clusters (MSCs). A magic-sized cluster is characterized as having a precise number of constituent atoms (it is a molecule) that leads to exceptional stability and distinct electronic, geometric, and chemical properties. As distinctive intermediates along the potential energy surface between precursors (i.e., atoms, ions, molecules) and nanocrystals, these clusters are crucial to unlocking a world of new possibilities in materials synthesis. They also offer a high-fidelity model of the structural complexity of nanocrystals, providing unique insights into the design of structure-function studies.

Examining the state of knowledge of nanoscale clusters, a stark contrast emerges between our understanding of metal clusters, exemplified by gold and silver and (binary) semiconductor clusters. With metals, our understanding has advanced considerably, allowing us to decipher the rules governing their possible sizes and atomic arrangements, ultimately granting us a level of predictive control^{1–4}. In metals, the atoms are arranged in well-defined, close-packed structures. As metals are downsized to the nanoscale, these close-packed structures persist, leading to the emergence of conserved structural motifs in metal nanoclusters, including icosahedra, decahedra,

and octahedra. Additionally, superatom theory explains that the magic-number stability observed in metal clusters results from forming closed-shell electronic orbital structures akin to noble gases^{5–8}. Semiconductor clusters, on the other hand, are a less explored frontier. The rules governing their structures remain elusive, leaving us uncertain regarding the full spectrum of possible atomic arrangements. Factors beyond the core stoichiometry, including surface chemistry, ion valency, and lattice covalency, likely significantly influence these structures⁹. The lack of structural predictability in semiconductor clusters has profound implications for our ability to harness their properties as we grapple with exploring uncharted territory and unlocking their untapped potential.

In this article, we will lay out our current understanding of the structure of II-VI and III-V semiconductor clusters that are isolated as intermediates in the synthesis of larger semiconductor nanocrystals and examine structural homologies between them. We will then look at several conversion reactions of semiconductor clusters, including cluster interconversions, atomistic seeded growth, and cation exchange. This reaction chemistry allows us to consider opportunities available for tuning the form and function of these clusters post-synthesis and isolation. It also opens additional possibilities to access entirely new cluster structures that have not (yet) been possible bottom-up.

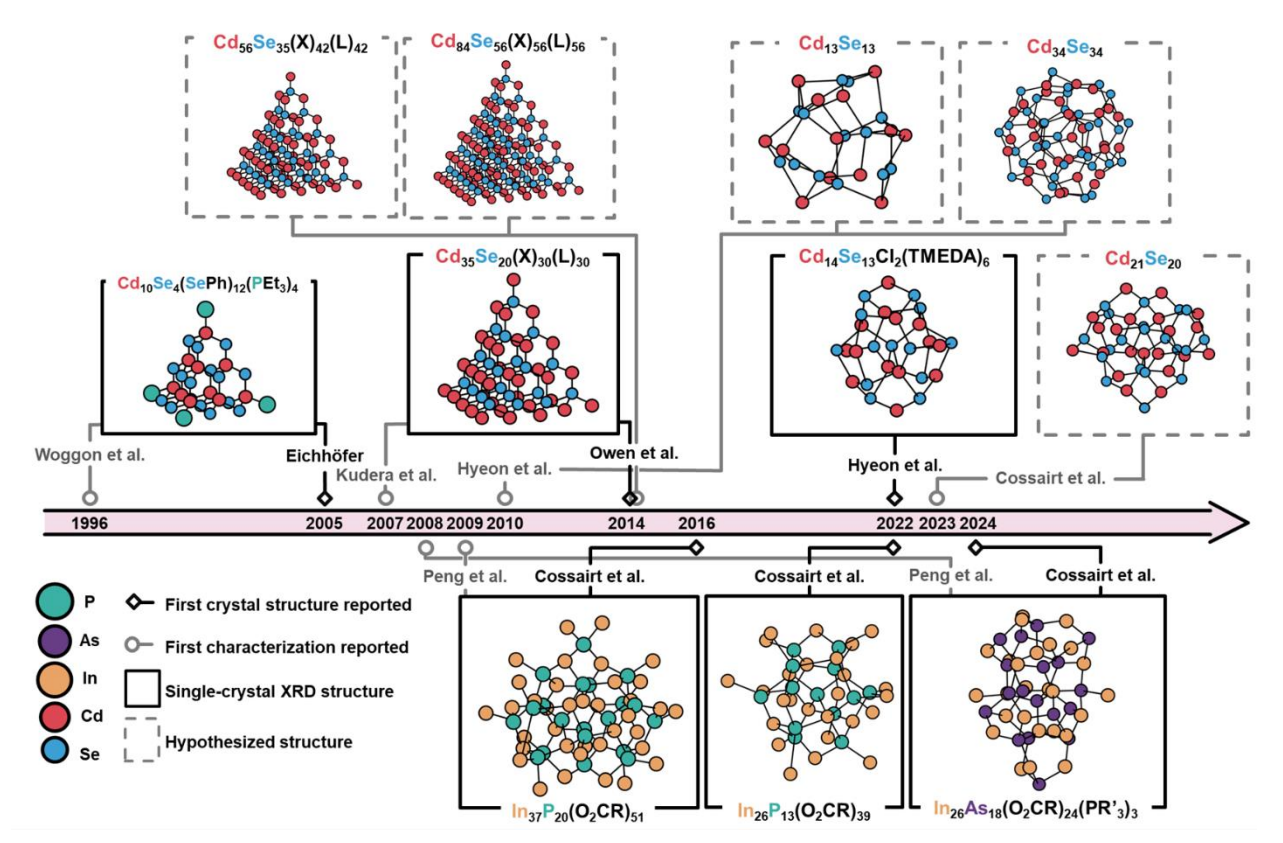


Figure 1: Timeline of discovery milestones for II-VI and II-V MSCs. For clarity, only the core of the clusters is shown. $X = O_2CPh$; $L = H_2N-C_4H_9$; $R = O_2CCH_2Ar$; R' = Et, Ph; TMEDA = tetramethylethylenediamine.

II-VI and III-V Clusters: Structure and Structural Homologies

II-VI Clusters

The existence of zincblende and wurtzite CdSe phases in the bulk hints at the possibility of "zincblende-like" and "wurtzite-like" CdSe MSC structures at the nanoscale. As the synthesis of these structures was first disclosed, theory was used to augment experimental observations to predict stable compositions $^{10-12}$. Further computational studies interrogated the electronic structure and surface chemistry of CdS and CdSe clusters $^{13-15}$. The first cadmium chalcogenide MSCs structurally characterized incorporated thiophenolates or selenophenolates into the inorganic core, resulting in MSCs with anion-rich compositions $^{16-19}$. Structural elucidation via single crystal X-ray diffraction showed an arrangement of cadmium and chalcogenide atoms in an extended adamantane-like structure reminiscent of zincblende CdSe or CdS (**Figure 1**, $Cd_{10}Se_4(SePh)_{12}(PEt_3)_4$).

More recently, CdSe MSCs with cadmium-rich core compositions were first synthesized by Manna and structurally characterized by Owen^{20,21}. A single crystal X-ray diffraction structure of the smallest isolable MSC in the series, featuring a lowest energy excitation maximum at 350 nm and core composition of Cd₃₅Se₂₀ (**Figure 1**), confirmed that the structure of this cluster is again zincblende-like with a tetrahedral morphology. In this case, the zincblende (111) facet is cadmium-rich, with undercoordinated cadmium passivated with benzoate and amine ligands. Additionally, two larger MSCs could be synthesized from Cd₃₅Se₂₀, with absorption maxima centered at 380 nm and 408 nm and inorganic core stoichiometries of Cd₅₆Se₃₅ and Cd₈₄Se₅₆, respectively (**Figure 1**). Pair distribution function (PDF) analysis of total X-ray scattering from these MSCs demonstrated that they maintain the zincblende-like core structure of Cd₃₅Se₂₀. Growth from one structure to the next-largest size occurs through the addition of a layer of Cd and Se monomers to one (111) facet of the zincblende tetrahedra, and Norris has extensively studied the theoretical framework for this mechanism²².

In addition to CdSe tetrahedral MSCs with cation-rich stoichiometries, more stoichiometric clusters, with core compositions of Cd₁₃Se₁₃ or Cd₁₄Se₁₃, were reported by Buhro and Hyeon towards the synthesis of two-dimensional nanomaterials^{23–26}. The structure of Cd₁₄Se₁₃ was disclosed by Hyeon in 2022 (**Figure 1**), highlighting its strikingly different structure from earlier reported MSCs²⁷. The quasi-spherical morphology arranges the Cd and Se atoms into a structure that resembles a highly strained wurtzite lattice. In particular, the central Cd and Se atoms are arranged vertically into eclipsed tetrahedra, which mirrors the bulk wurtzite structure. However, the cations and anions also twist from this vertically stacked arrangement to accommodate the geometric constraints of the small size. Intriguingly, structural similarities between the single-crystal structures of Cd₁₄Se₁₃ and In₂₆P₁₃²⁸ characterized by single-crystal X-ray diffraction point to the possibility of further homology between the II-VI and III-V MSCs (**Figure 2A**). In

particular, the $In_{37}P_{20}$ cluster (**Figure 1**), characterized as possessing a pseudo-wurtzite structure through single crystal X-ray diffraction by our lab²⁹, presents the possibility that there is a larger CdSe MSC with the same structure.

The literature has ample precedent for these "wurtzite-like" CdSe MSCs. Rosenthal has extensively worked on stoichiometric MSCs and "ultrasmall" quantum dots (QDs) with a lowest energy absorption feature at approximately 420 nm and a wurtzite structure observed by TEM³⁰. Similarly, Kasuya¹⁰, Hyeon^{25,27}, Buhro²⁴, Sardar³¹, and Owen³² have reported an MSC with a reported core stoichiometry of Cd₃₃Se₃₃, Cd₃₄Se₃₃, Cd₃₄Se₃₄, or Cd₃₅Se₂₈ and the same absorption maximum as the Rosenthal studies at approximately 420 nm. We hypothesized that these reports represent the same structure, with different synthesis conditions or characterization procedures resulting in the observed compositional differences. To support this hypothesis, we proposed that a large-scale, reproducible synthesis would allow us to characterize the structure of this MSC more definitively. Furthermore, if we utilized the same ligands as those in the synthesis of a zincblende MSC, we could contrast the inorganic core structures of the two polymorphs more effectively.

We found that both cation-rich, zincblende MSCs, and stoichiometric, wurtzite-like MSCs could be accessed from identical precursors by controlling reagent stoichiometry³³. The addition of an equimolar amount of diphenylphosphine selenide (DPPSe) to in situ generated cadmium benzoate yielded an MSC with a characteristic absorption maximum at 420 nm in the UV-Vis spectrum that we proposed possessed a core composition of Cd₂₁Se₂₀. Alternatively, using only 0.5 equivalents of DPPSe in the synthesis produced a cluster with absorption features consistent with the cationrich MSC Cd₃₅Se₂₀ that was first structurally characterized by Owen²¹. While elemental analysis and powder X-ray diffraction are useful techniques in initially distinguishing compositional and structural features between these two MSC classes, we found pair distribution function (PDF) analysis of total X-ray scattering to be the most insightful technique in assigning the structure of this cluster with absorption maximum of 420 nm. The reduced PDF G(r) is a probability distribution of interatomic distance pairs found in the cluster, and we can attribute peaks in G(r)as Cd-Se, Cd-Cd, and Se-Se interatomic distances to support a structural assignment. The experimental PDF of the MSC has a broad peak at approximately 4 Å that corresponds to the distribution of Cd-Cd and Se-Se distances found in the structure (Figure 2B). This is contrasted with the simulated PDF of Cd₃₅Se₂₀, which features a series of sharp peaks consistent with the more periodic zincblende-like structure. Furthermore, we could state the diameter of this cluster was tentatively larger than Cd₁₄Se₁₃ (with a size of 0.9 nm²⁷) based on the extended oscillations of G(r) past 10 Å.

This structural analysis from the PDF allowed us to propose that the cluster is a larger, stoichiometric cluster within the same pseudo-wurtzite structural family as Cd₁₄Se₁₃. We then demonstrated that Cd₂₁Se₂₀ and the InP MSC In₃₇P₂₀ are homologous structures by generating a structural model from the In₃₇P₂₀ single crystal structure²⁹. Swapping In and P atoms for Cd and

Se atoms yielded a $Cd_{37}Se_{20}$ composition ($Cd_{21}Se_{20}$ core with 16 surface Cd^{2+} ions, *vide infra*). In the simulated PDF, this structure matches the peak intensities, peak positions, and MSC size of the experimental PDF of the cluster. Since elemental analysis *via* ICP-OES of our cluster samples shows a stoichiometric composition of Cd: Se = (1.02 ± 0.06) :1³³, we proposed a formula of $Cd_{21}Se_{20}$ that matches the core of $In_{37}P_{20}$ (**Figure 2C**).

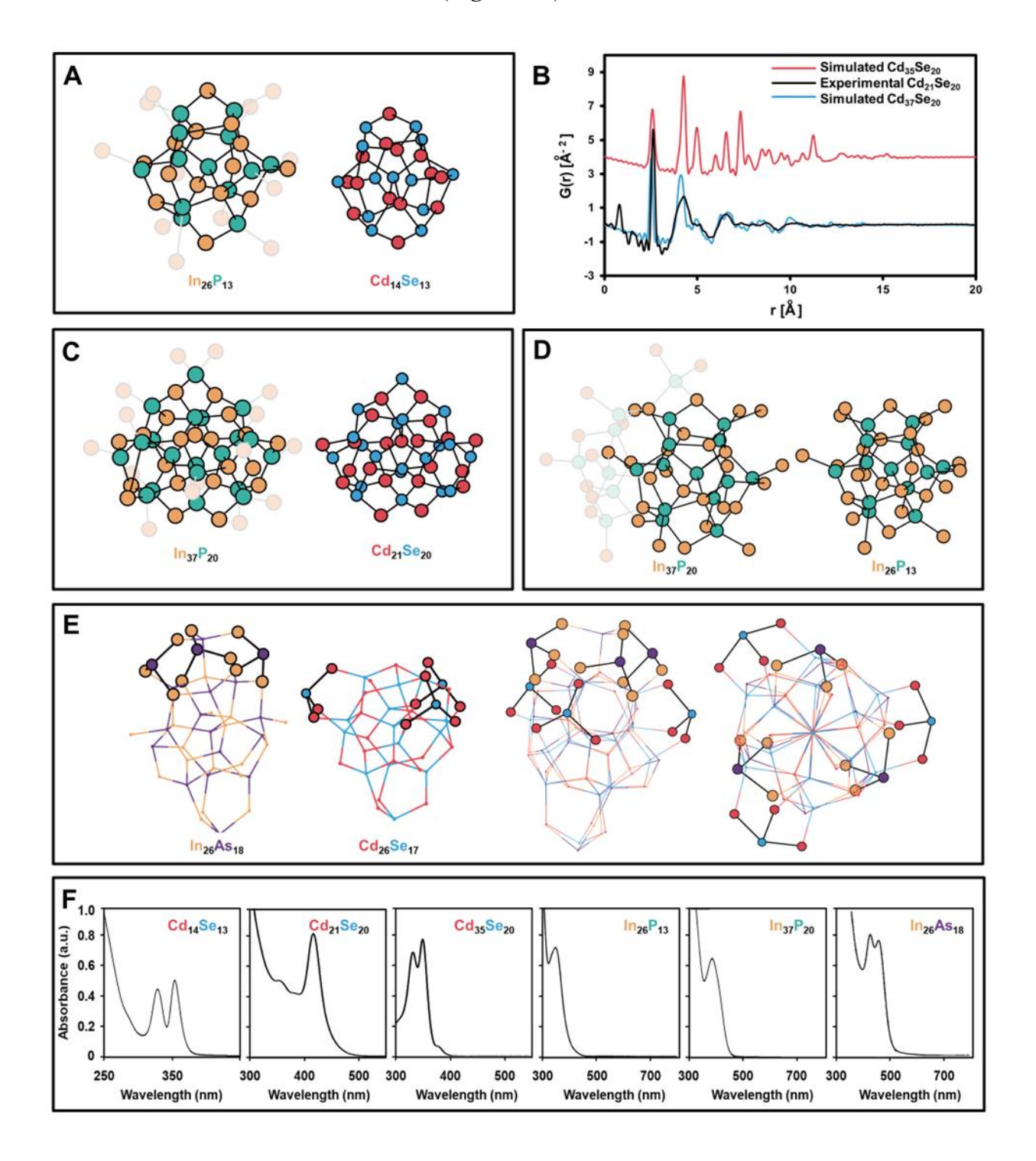


Figure 2: Structural homology across III-V and II-VI magic-sized clusters. A) Comparison of the structures of In₂₆P₁₃ and Cd₁₄Se₁₃. The core structures of In₂₆P₁₃ and Cd₁₄Se₁₃ are the same. B) Comparison of PDF analysis of the experimental G(r) of Cd₂₁Se₂₀, the simulated *G(r)* of Cd₃₅Se₂₀, and the simulated *G(r)* of Cd₃₇Se₂₀. Adapted with permission from reference 33. Copyright 2023 American Chemical Society. C) Comparison of the structure of In₃₇P₂₀ and the proposed structure of Cd₂₁Se₂₀, which was generated from the stoichiometric core of In₃₇P₂₀. D) Comparison of the structures In₃₇P₂₀ and In₂₆P₁₃. In₂₆P₁₃ is a subunit of the larger cluster In₃₇P₂₀. E) Comparison of the structure of In₂₆As₁₈ and the structure of Cd₂₆Se₁₇. F) UV-vis absorption spectra of II-VI and III-V clusters. Adapted with permission from reference 27, copyright 2022 Cell Press (Cd₁₄Se₁₃); reference 33, copyright 2023 American Chemical Society (Cd₂₁Se₂₀ and Cd₃₅Se₂₀); reference 28, copyright 2024 American Chemical Society (In₂₆P₁₃ and In₃₇P₂₀); reference 48, copyright 2024 American Chemical Society (In₂₆As₁₈); and reference 49, copyright 2023 Springer Nature (Cd₂₆Se₁₇).

III-V Clusters

The first synthesis of an InP cluster came from Peng in 2009 by reacting indium carboxylate, the corresponding carboxylic acid, and tris(trimethylsilyl)phosphine (P(SiMe₃)₃) at a variety of temperatures in the range of 100 - 200 °C³⁴. The persistence of a nanocluster across a range of temperatures in the InP system suggested that the thermodynamic favorability of nucleation events doesn't necessarily control the mechanism of nanocrystal growth. Instead, the high reactivity and solute concentration lead to no thermodynamic barrier until these discrete atomically precise clusters are formed. This presented the importance of considering nonclassical nucleation procedures in III-V nanocrystal systems. Our group continued the investigation of this molecule as a single source precursor, showing that it could generate InP QDs with a competitive degree of monodispersity^{35,36}. This ultimately led to synthesizing the InP clusters using phenylacetate ligands that imparted a high enough surface rigidity to allow for single crystal growth and complete structural characterization³⁷. This unveiled the $In_{37}P_{20}(O_2CR)_{51}$ stoichiometry wherein a $[In_{21}P_{20}]^{3+}$ core is passivated by 16 In³⁺ and 51 carboxylate anions, resulting in a neutral overall structure. The pseudo-wurtzite core contains interlinked, repeating polytwistane InP units. While made up of tetrahedral In₄P units similar to the wurtzite and zincblende bulk structures, the arrangement of these units is much less symmetrical, as evidenced by the C₂ rotation axis. A view down the C₃ axis of surface In₄P units does show the inverted tetrahedron behavior of wurtzite more closely than the repeated tetrahedral symmetry of zincblende, but these units twist towards the center of the molecule, making it far from traditional wurtzite. The structure also allowed for further insight into the surface of the nanocluster, showing complete passivation by carboxylate ligands represented in 4 different binding modes: chelating, asymmetric bridging, symmetric bridging, and chelating + dative. The surface was further probed in a subsequent study using FTIR and transient IR spectroscopy to show that the binding mode distribution is altered in solution and that all ligands

are strongly coupled to excitons generated within the cluster³⁸. Subsequent studies investigated surface ligand exchange chemistry³⁹, cation exchange^{40,41}, and the seeded growth of larger metastable pseudo-wurtzite QDs⁴².

In general, it has been proposed that carboxylate-ligated In₃₇P₂₀ clusters have conserved core connectivity for different ligands based on their consistent optical and spectroscopic properties. However, it was documented that the ³¹P NMR resonances were responsive to the tail of the carboxylate, be it myristate, oleate, or phenylacetate²⁹. This suggested that the external pressure of the ligand sphere could influence the internal structure of the In₃₇P₂₀ core. We then sought to document and further characterize the structural responses of the InP core to a standardized framework of carboxylate ligands. To this end, the In₃₇P₂₀(O₂CR)₅₁ cluster was synthesized with phenylacetate (PhAc) ligands as well as 4-*tert*-butylphenylacetate (tBu), *m*-tolylacetate (3-Me), and 3,5-dimethylphenylacetate (3,5-Me₂) ligands allowing for an analysis of how the core responds to para-substitution as well as an increasing degree of meta-substitution.²⁸ We also noted that using *o*-tolylacetate allowed for transient cluster formation before destabilization and loss of colloidal stability, while 3,5-di-*tert*-butylphenylacetate appeared to bypass cluster formation to generate colloidally stable QDs.

The ³¹P NMR resonances were descriptive for individual phosphorus environments, showing the bulkiness of the 4-tBu group induced a significant shift in the resonance of the most downfield, apical phosphorus atom as well as a variety in partial coalescence and symmetry breaking of other resonances. Meta-substitution, however, increased the line broadness, thereby hampering the interpretation of specific ³¹P shifts. Nonetheless, this broadening was interpreted through the lens of structural rigidity, which can modify the relaxation time of nuclei, leading to similar line broadening results.⁴³ Raman spectroscopy further corroborated the rigidification, showing that the surface pressure of the meta-substituents dampened specific Raman-active vibrations of the InP core. This was also observed with the 4-tBu ligation, but to a lesser extent, likely because the substituent imparting rigidity is directed away from the cluster's surface. The structural perturbations were further corroborated by PDF analysis showing ligand-dependent shifts in the average In-P bond distances, In-In separation distances, and even longer-range core-surface correlations near 10 Å.

While synthesizing the library of In₃₇P₂₀ clusters, we found that the procedure used to form the indium carboxylate in the case of the 4-tBu ligand was vital for the result of the synthesis. Reacting indium (III) acetate and a slight excess of 4-*tert*-butylphenylacetic acid to generate the carboxylate resulted in a product morphology that was not entirely soluble in toluene at the reaction temperature. Introducing P(SiMe₃)₃ resulted in the characteristic absorbance feature at 386 nm of the In₃₇P₂₀ cluster. However, forming the indium carboxylate through the direct reaction of trimethylindium and 4-*tert*-butylphenylacetic acid resulted in a soluble precursor at room temperature. The reaction of this precursor with P(SiMe₃)₃ resulted in a sharp absorbance feature at 350 nm. Structural characterization by SCXRD proved this new species to be In₂₆P₁₃(O₂CR)₃₉.

Structural comparison between $In_{26}P_{13}$ and $In_{37}P_{20}$ showed a very small root mean squared deviation value, proving a large amount of structural overlap between the two structures (**Figure 2D**). When aligned with a similar synthetic route, this fact strongly suggests that $In_{26}P_{13}$ formation precedes $In_{37}P_{20}$ formation in the indium carboxylate and $P(SiMe_3)_3$ system. More detailed consideration of the $In_{26}P_{13}$ structure showed that it was homologous to a recently isolated $Cd_{14}Se_{13}$ cluster from the Hyeon group (**Figure 2A**) but had a significantly more cation-rich surface directed by the apparent 4-coordinate requirement of phosphorus. Seeing that $In_{26}P_{13}$ formation precedes that of $In_{37}P_{20}$ and there are strong structural similarities between $In_{26}P_{13}$ and $Cd_{14}Se_{13}$, this would suggest that the $Cd_{21}Se_{20}$ cluster documented from the growth of $Cd_{14}Se_{13}$ is the stoichiometric equivalent of the $In_{37}P_{20}$ cluster²⁷.

After structurally identifying some of the intermediates in the InP system, we sought to expand our study to a similar but less developed nanomaterial system, InAs. Previously reported syntheses of InAs QDs are similar to those for InP but use indium carboxylate, tris(trimethylsilyl)arsine, and include a tertiary organophosphine such as trioctylphosphine (TOP)^{44–47}. Similar to InP, atomically precise clusters were observed as persistent intermediates in the synthesis of InAs QDs.^{44–47} While many reports of high-quality InAs QDs optically reported the presence of the cluster, there was very little characterization of the intermediate itself. Seeing as the InP crystal structure allowed for many further studies and insights into the InP nanocrystal mechanism, we sought to accomplish complete structural characterization of the InAs cluster.

Employing indium phenylacetate and diethylphenylphosphine in toluene at 110 °C, the injection of tris(trimethylsilyl)arsine resulted in InAs clusters with a ligand sphere rigid enough to allow for single-crystallization by vapor diffusion⁴⁸. This provided the assignment In₂₆As₁₈(O₂CR)₂₄(PR')₃ and showed the cluster structure to be quite different from other reported semiconductor cluster structures. Within the III-V material family, the P sublattice of the In₂₆P₁₃ cluster we reported previously overlaps with the As sublattice of the In₂₆As₁₈. Despite that, there is very little similarity in the arrangement of the In atoms between the two structures. This is likely due to the seven 3-coordinate As atoms, which drastically reduces the cation-richness of the cluster and sets it apart from its InP counterparts, in which all P atoms are 4-coordinate. This decrease in cation richness results in a substantial reduction in ligand coverage at the cluster surface, allowing for elevated reactivity through uninhibited diffusion of reactants to the cluster surface.

Expanding structural comparisons to other materials shows a surprising degree of structural overlap with a recently reported Cd_26Se_{17} cluster synthesized through complete cation exchange of $Cu_26Se_{13}^{49}$ (**Figure 2E**). The underlying $M_{17}E_{14}$ cage substructure is homologous between the two clusters, but the attachment of the three additional M_3E units in the CdSe cluster occurs at the lower half of the cage, to generate a pseudo-tetrahedron whereas in the InAs cluster, these units add to the base generating an anisotropic bullet-like morphology. Seeing as another InAs cluster precedes the formation of $In_{26}As_{18}$ through an isosbestic point, its structure is of particular interest as it could provide further information as to the growth pathways and attachment of InAs units.

Conversion and Reactivity of II-VI and III-V Clusters

While magic-sized clusters have been observed as intermediates in the synthesis of QDs for several decades^{50,51}, manipulating these structures could allow access to truly monodisperse nanocrystalline products or to otherwise inaccessible phases. With the elucidated structures of II-VI and III-V clusters in hand, our lab was interested in probing some of these methods of control. We postulated that magic-sized clusters allow for phase control through interconversion reactions, controlled growth into larger quantum dots, and a controllable composition using ion exchange.

Cluster Interconversion

Control of II-VI cluster reactivity in an atomically precise manner has been recently demonstrated under various contexts *via* ligand exchange, facet-dependent layer-by-layer growth, and cation exchange. For example, Robinson and coworkers disclosed an isomerization reaction between two CdS MSCs that is triggered by surface methanol adsorption⁵². Similarly, Hyeon and coworkers prompted the growth of Cd₁₄Se₁₃ into a larger cluster *via* tertiary amine to primary amine ligand exchange²⁷. Kudera first reported controlled and discrete growth of CdSe MSCs, which Norris and coworkers expanded on through a mechanistic understanding of layer-by-layer growth on zincblende (111) facets.^{20,22} Separately, Yu and coworkers proposed a two-step model for the isomerization and interconversion of MSCs that involves optically transparent "precursor compounds" as an intermediate between clusters⁵³. In a series of literature reports, the authors demonstrated the temperature-controlled, reversible isomerization of CdS MSCs⁵⁴, the growth of several CdSe⁵⁵ and CdTe⁵⁶ MSCs from a single CdE precursor mixture, and the growth of CdSe MSCs after cadmium acetate addition to ZnSe clusters⁵⁷.

With these precedents in mind, we questioned whether we could toggle between the two known CdSe MSC phases to controllably yield either zincblende-like or pseudo-wurtzite MSCs from the opposite structure motif (**Figure 3A**). Towards this goal, we found that adding cadmium or selenium precursor promoted this rearrangement, with precursor concentration directly correlated with conversion rate and extent of conversion³³. Starting with the pseudo-wurtzite cluster Cd₂₁Se₂₀, the addition of excess cadmium benzoate resulted in the formation of zincblende-like tetrahedra. The formation of these tetrahedra is observed by UV-vis absorption spectroscopy while monitoring the reaction over twenty minutes, with a decrease of the absorbance maximum of Cd₂₁Se₂₀ at 420 nm occurring concurrently with an increase in peaks consistent with the formation of Cd₃₅Se₂₀, Cd₅₆Se₃₅, Cd₈₄Se₅₆, and additional larger tetrahedra (**Figure 3B**). We then confirmed that these absorption peaks corresponded to the proposed tetrahedra by isolating them with size-selective precipitation.

Structural analysis of the resulting products was accomplished using PDF analysis of total X-ray scattering, which demonstrated the conversion reaction produced a new structure type (**Figure 3C**). The interatomic distances and peak intensities in the experimental PDF of Cd addition to Cd₂₁Se₂₀ are strikingly similar to the simulated PDF of the tetrahedron Cd₃₅Se₂₀. This close match highlights that the product sample is now zincblende-like. However, extended correlations in the experimental PDF to 20 Å contrast with the end of correlations in the simulated PDF of Cd₃₅Se₂₀ at 13 Å. These additional longer-range correlations imply that the structure has grown, consistent with the appearance of red-shifted UV-vis absorption peaks over the reaction corresponding to the discrete growth of larger tetrahedra.

Having demonstrated the conversion from pseudo-wurtzite to zincblende structure, we asked whether the opposite reaction could also proceed, allowing for the synthesis of either polymorph from the opposite structure. We found that adding excess diphenylphosphine selenide (DPPSe) to the zincblende-like tetrahedron Cd₃₅Se₂₀ resulted in full consumption of the original cluster. Reaction monitoring with UV-vis absorption spectroscopy showed a gradual redshift and increase in intensity at approximately 420 nm over the course of the hour (Figure 3D). Further investigation of the reaction kinetics demonstrated a linear increase in the absorbance intensity at 420 nm as a function of the concentration of DPPSe. While this does not necessarily imply that the exact structure of Cd₂₁Se₂₀ is synthesized under these conditions, we hypothesized that a different cluster with changed core composition resulted from adding excess selenium to the original zincblende structure. This hypothesis was corroborated by comparing the simulated PDF of Cd₃₅Se₂₀ to the experimental PDF of isolated products from adding excess DPPSe (Figure 3E). While the experimental PDF has lost many of the sharp peaks characteristic of the zincblende structure type observed in Cd₃₅Se₂₀ (Figure 3D), the experimental PDF overlays with the experimental PDF of Cd₂₁Se₂₀ and closely matches the peak positions and intensities. These results demonstrate that adding selenium precursor to the zincblende MSC results in an internal atomic structure that mimics Cd₂₁Se₂₀ – the pseudo-wurtzite phase.

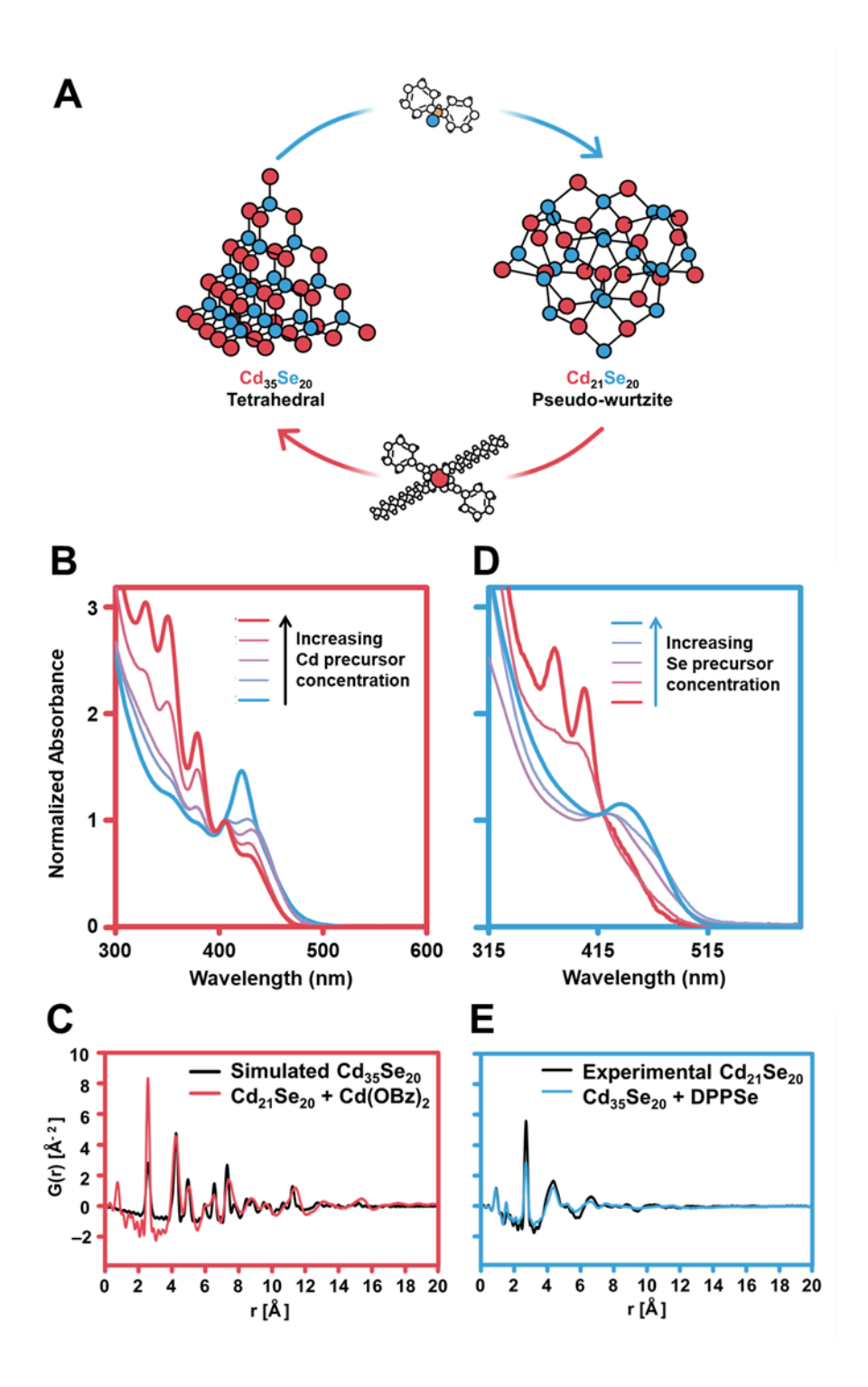


Figure 3: Interconversion of CdSe MSC polymorphs. Adapted with permission from reference 33. Copyright 2023 American Chemical Society. A) Adding excess cadmium benzoate to the pseudo-wurtzite MSC Cd₂₁Se₂₀ produces a series of zincblende tetrahedra. Adding excess diphenylphosphine selenide to the zincblende-like cluster, Cd₃₅Se₂₀ yields a pseudo-wurtzite

structure. B) Reaction monitoring *via* UV-vis absorption spectroscopy of cadmium benzoate addition to $Cd_{21}Se_{20}$ with increasing concentration of Cd precursor (20-minute timepoint shown). C) Comparison of PDF analysis of experimental G(r) of Cd precursor addition to $Cd_{21}Se_{20}$ and simulated G(r) of $Cd_{35}Se_{20}$. D) Reaction monitoring *via* UV-vis absorption spectroscopy of diphenylphosphine selenide addition to $Cd_{35}Se_{20}$ with increasing concentration of Se precursor (60-minute timepoint shown). C) Comparison of PDF analysis of experimental G(r) of Se precursor addition to $Cd_{35}Se_{20}$ and experimental G(r) of $Cd_{21}Se_{20}$.

Growth

Since the In₃₇P₂₀ cluster functions as an intermediate in the synthesis of InP QDs, we are generally interested in investigating how the cluster functions in that role and as a single-source precursor. Our group's initial efforts to employ In₃₇P₂₀ clusters as single-source precursors showed that at high temperatures (400 °C), the injection of isolated clusters resulted in high-quality InP QDs³⁵. The size of the resulting nanocrystals could be controlled through the cluster concentration upon injection. Further investigation of the conversion showed that temperatures as low as 200 °C could induce cluster destabilization, nucleation, and eventually the growth of QDs³⁶. However, extended heating below this temperature regime resulted in slow decomposition with no productive growth of nanocrystals. Concentration and temperature were confirmed to alter the conversion rate as well as exogenous additives such as excess carboxylic acid and indium carboxylate. These kinetic studies indicated a potential surface dependence on the rate of nanocrystal growth upon cluster dissolution.

After synthesizing $In_{37}P_{20}$ clusters using ligands with various steric profiles, we sought to analyze their behavior of clusters as single source precursors through hot injection thermolysis at 240 °C²⁸. This study showed that the surface chemistry could impact the size of the nanocrystals grown from cluster thermolysis. The size trend observed suggested that the steric profile and its influence on diffusion was the primary variable responsible for altering nanocrystal size. We concluded that a larger steric profile hinders solute diffusion, which is responsible for growth. This leads to an inflated solute concentration with bulkier ligands that extend the nucleation period, resulting in smaller nanocrystals.

After observing differences in nucleation and growth rates through thermolysis, we were also interested in potentially leveraging the structural perturbations in the In₃₇P₂₀ cluster to investigate how those may impact surface reactivity. This was spurred on by computational work from Kulik and coworkers showing the separation distances between surface indium atoms could modulate the reactivity towards active phosphines⁵⁸.

Building from previous work in our group showing that subjecting the In₃₇P₂₀ clusters to further equivalents of P(SiMe₃)₃ resulted in the growth of larger pseudo-wurtzite nanocrystals, we

monitored the kinetics of cluster to QD conversion through this pathway to investigate any ligand dependence. Previously, we discovered that the addition of 5-15 eq of $P(SiMe_3)_3$ to isolated $In_{37}P_{20}$ clusters resulted in fragmentation of the atomically precise material followed by the templated growth of the thermodynamically-trapped pseudo-wurtzite phase of the cluster⁴². This occurred at modest temperatures (40 - 100 °C) and was brought about by the silyl groups irreversibly stripping carboxylate ligands from the cluster's surface forming silyl ester coproducts. It was also found that fewer equivalents of $P(SiMe_3)_3$ (1 - 2 eq) caused fragmentation into a new, distinct atomically precise cluster that we posited functioned as a critical intermediate in the higher equivalent reactions. Through the distinct ^{31}P NMR resonances, we could later assign this intermediate as the $In_{26}P_{13}$ cluster discussed above. As this conversion process is severely surface-dependent due to the necessary carboxylate removal, we sought to use it as a framework for studying the reactivity of our library of $In_{37}P_{20}$ clusters.

By subjecting the library of In₃₇P₂₀ clusters to 10 eq of P(SiMe₃)₃ at 40 °C and monitoring the increase in absorbance at 500 nm over time, we were able to track the conversion from cluster to larger nanocrystals (Figure 4A). These conversions could then be fit to an exponential and compared across ligands to quantitatively assess the conversion rates (Figure 4B). This analysis showed that the 4-tBu cluster was the least reactive, followed by PhAc, which was less reactive than 3-Me, and finally, 3,5-Me₂ was the most reactive. We interpreted this trend through three possible variables that could impact reactivity. Firstly, the steric profile, through the addition of substituents, hinders phosphine diffusion to the surface. Second, as predicted by Kulik and coworkers, changing the indium separation distances on the surface can alter the reactivity⁵⁸. Finally, stacking of the phenyl groups on the surface of the cluster can cause the carboxylates to become more labile, thereby augmenting the reactivity. Applying these interpretations to the experimental rates, the tert-butyl para-substituent had a powerful impact on modulating the diffusion of P(SiMe₃)₃ through the ligand sphere, making it the least reactive. In contrast, increasing the number of meta-substituents, to some extent, hinders diffusion, but the main effects come from these substituents directing phenyl group stacking and shortening the indium separation distances on the surface. This increased the reactivity of the cluster with P(SiMe₃)₃, where additional meta-substituents made the surface more reactive. The phenylacetate cluster functioned as a control where its reactivity was greater than 4-tBu but less than 3-Me. This emphasizes the importance of surface chemistry in controlling cluster properties and suggests that the behavior of clusters as an intermediate in the synthesis of QDs may be controlled by ligand behavior.

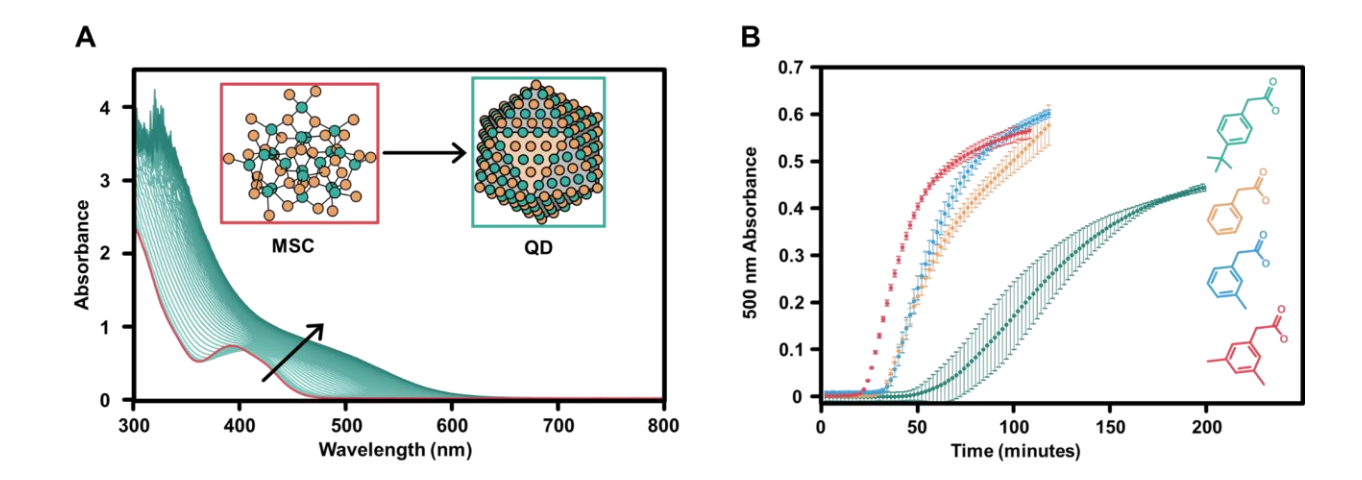


Figure 4: A) Example of a conversion from 3-Me In₃₇P₂₀ clusters into InP QDs monitored by UV-Visible absorption spectra with P(SiMe₃)₃ addition from 0 min (red) to 118 min (green). B) Absorbance at 500 nm over time after addition of 10 eq of P(SiMe₃)₃ to In₃₇P₂₀ clusters with different phenylacetate ligands (green: 4-tBu phenylacetate, orange: phenylacetate, blue: 3-Me phenylacetate, red: 3,5-Me₂ phenylacetate). Adapted with permission from reference 28. Copyright 2024 American Chemical Society.

Ion Exchange

As magic-sized clusters serve as molecularly precise analogs to larger nanomaterials, they are excellent platforms for studying complex post-synthesis reactions to give further insight into the underlying principles and more rational design. While we have previously described the use of clusters to examine ligand binding^{39,59} and nucleation of larger nanoparticles,²⁸ other primary reactions of interest are cation and anion exchange. Cation exchange is a post-synthetic reaction that transforms one nanoparticle to another with similar size, shape, and even crystal structure but with new compositions and properties (**Figure 5A**). Cation exchange reactions are beneficial for making materials that are difficult or impossible to make bottom-up.

Partial cation exchange (also known as doping) has been widely reported for CdS(e) MSC species. These studies generally examine the new magnetic properties imparted by introducing a magnetic dopant such as Mn²⁺ or Co²⁺.60-64 These studies have shown that incorporating one Mn²⁺ ion to the Cd₁₃Se₁₃ cluster leads to giant Zeeman splitting, while clusters with multiple Mn²⁺ are magneto-optically inactive.^{61,62} Co²⁺ can be incorporated up to 10% (two Co²⁺ ions) in two four-fold selenium-coordinated sites.⁶³ In CdS and ZnS cluster analogs, Co²⁺ was found to substitute rapidly in smaller cluster species. In comparison, substitution in larger cluster analogs took much longer due to the fast ligand interconversion in the smaller species.^{64,65} Mn²⁺ was found to vary its incorporation site depending on the stage that the Mn²⁺ is added to the cluster; at early time points in the cluster synthesis, the Mn²⁺ incorporates into the core, while post-synthetic addition of Mn²⁺ leads to surface incorporation of Mn²⁺.⁶⁶

Alternatively, anion exchange has been demonstrated under certain conditions using II-VI cluster systems. For example, Yu and coworkers showed that mixing amorphous samples of CdSe and CdTe forms a CdTeSe MSC with sharp absorption features. More recently, Wang and coworkers disclosed a protocol for complete anion exchange between cadmium chalcogenide clusters that proceeds through disordered intermediates and with a reaction mechanism that depends on the stoichiometry of the cluster.

Despite this previous work examining II-VI-based clusters, our group was the first to investigate InP MSCs as a platform for cation exchange, specifically the conversion of InP MSC to a well-defined cadmium phosphide cluster. ⁴⁰ By introducing varying amounts of cadmium precursor, we were able to collect a series of intermediates between InP MSCs and ultrasmall Cd₃P₂ and observe the reaction pathway of the cluster via a variety of analytical methods (pXRD, XPS, UV-Vis absorbance, PDF, ³¹P NMR, and MS). It was found that in this series of exchange reactions, the MSCs first undergo a topotactic exchange, initially replacing the surface-bound In-carboxylates. Upon introducing more Cd to the cluster, we observed the diffusion of Cd into the previously untouched core, followed by a final conversion event. The complete exchange is reminiscent of the cooperative ion exchanges in the CdS(e) lattices upon the introduction of Cu or Ag. ^{68–70}

These results were further expounded, with an interest in incorporating other cations, such as isovalent Ga³⁺ and aliovalent Zn²⁺.⁷¹ Our group demonstrated that the Zn ions readily incorporate in InP MSCs at room temperature, but Ga ions resist incorporation beyond the surface. However, using a highly reactive precursor, [Ga(NMe₃)₂]₂, increased the concentration of Ga associated with the MSC. In the case of both Zn and Ga, we observed an exchange reaction similar to Cd, in which the surface undergoes a non-site selective topotactic exchange. These materials were then utilized in a hot injection reaction to grow larger nanocrystals to determine if QDs prepared from doped clusters would show enhanced optical activity compared to surface-treated QDs. When using the Zn-doped clusters, the resultant QDs showed significant blue shifts in the absorbance spectra and increased photoluminescence quantum yield relative to the amount of Zn added to the cluster. Interestingly, the pXRD of these materials did not show shifts to higher two theta that would be expected for alloyed QDs, indicating that the Zn doping is likely limited to the outer layers of the InP core. This suggests that the increase in photoluminescence quantum yield (PLQY) arises from in situ Zn treatment of InP, passivating trap sites.⁷² The Ga-doped QDs synthesized from the treated clusters showed slight redshifts in the absorbance spectra and exhibited the zinc-blende InP phase via pXRD, indicating surface association of the Ga atoms similar to the Zn-treated samples. However, these materials did not exhibit increased PLQY, suggesting that surface Ga treatment of InP QDs is insufficient to passivate intrinsic trap states.

More recent work in our group has detailed the conversion of InP MSCs to Cu_{3-x}P, Ag_{3-x}P, and Au_{3-x}P clusters.⁴¹ We observed that this reaction is driven by the introduction of amine to MSC solutions in the presence of a coinage metal salt. The amine is proposed to remove a small amount of the surface indium, causing a cluster rearrangement.⁷³ Not only does this rearrangement reduce

the ligand density, allowing for easier access of dopant cations to the cluster surface, but it also causes the resultant cluster to be less stable and more likely to interact with dopant cations. ^{58,74,75} This rearrangement can be monitored by tracking the changes in the steady state and transient optical spectroscopy. The cation of choice can then interact with the cluster, causing distortion in the lattice, observable via higher angle shifts and broadening in the pXRD, with equivalents driving the reaction to form new crystal structures. These new structures were probed via PDF and XPS analysis finding the complete extrusion of indium ions, with any remaining indium functioning as loosely associated In-carboxylate. Similarly to the Zn and Ga treated samples, the conversion of these doped clusters leads to the formation of doped InP QDs. However, unlike the Zn and Ga samples, the coinage metals were incorporated into the core of the resultant QD, leading to characteristic broadened absorption features and NIR emission. Upon hot injecting the fully converted clusters, we observed the formation of larger nanoparticles of Cu_{3-x}P and the novel nanophases of Ag_{3-x}P and Au_{3-x}P.

This work emphasizes the utility of MSCs as cation exchange platforms. The homogeneity of MSCs allows for precise determination of cation exchange mechanisms, and the intrinsic metastable nature of these materials also allows for the formation of phases that would be highly difficult to obtain via traditional synthetic methods.

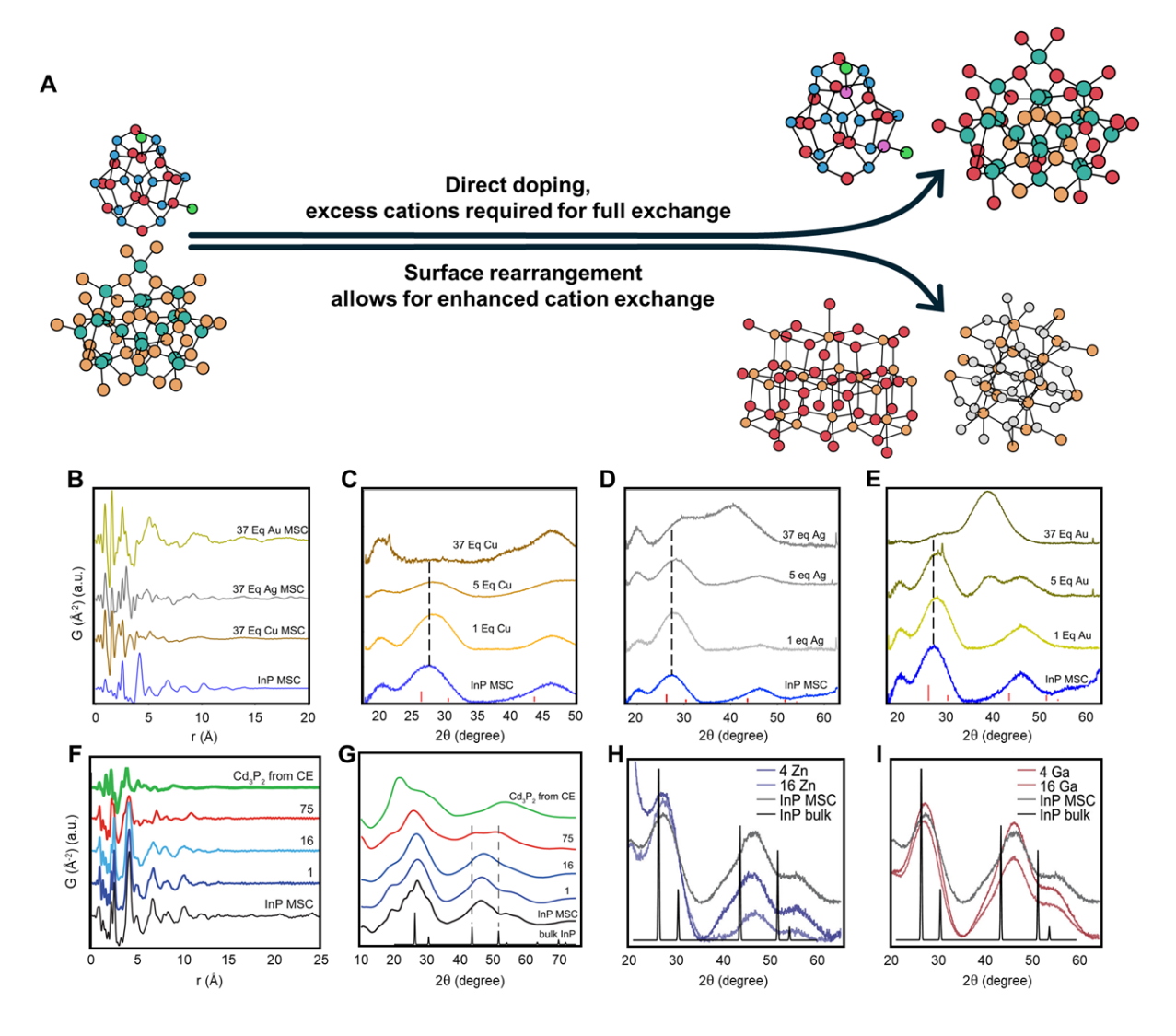


Figure 5: A) Schematic illustration showing examples of direct, topotactic doping of MSCs (top) and cation exchange mediated by surface exchange and rearrangement (bottom). PDF (B) and pXRD (C-E) of coinage metal (Cu, Ag, Au) cation exchange in In₃₇P₂₀ MSCs. Adapted with permission from reference 41. Copyright 2024 American Chemical Society. PDF (F) and pXRD (G) of Cd²⁺ cation exchange in In₃₇P₂₀ MSCs. Adapted with permission from reference 40. Copyright 2017 American Chemical Society. pXRD of In₃₇P₂₀ MSCs treated with Zn²⁺ (H) and Ga³⁺ (I). Adapted with permission from reference 71. Copyright 2019 AIP Publishing.

Conclusions and Outlook

Our exploration into the structure and reactivity of II-VI and III-V MSCs has unveiled significant structural homologies between the semiconductor families, marking a step forward in our understanding of nanoscale materials. These homologies bridge the gap between II-VI and III-V semiconductor clusters, drawing a fascinating parallel to the bulk zinc blende and wurtzite phases

and underscoring our ability to transcend conventional constraints of thermodynamic stability at these smallest size scales (Figure 6). Specifically, three III-V clusters have been identified and our structurally characterized team: $In_{37}P_{20}(O_2CR)_{51}$, $In_{26}P_{13}(O_2CR)_{39}$ In₂₆As₁₈(O₂CR)₂₄(PR')₃. All three of these clusters contain a pseudo-wurtzite cluster core. In₃₇P₂₀ and In₂₆P₁₃ are proposed to be on the same reaction coordinate and represent individual members of this InP cluster family. In₂₆P₁₃ is also structurally homologous with Cd₁₄Se₁₃, with the only difference being the surface anion termination where all 13 anions are completely tetrahedrally coordinated by cations in the case of the InP cluster. We propose that the well-known CdSe-420 cluster, which can be produced from Cd₁₄Se₁₃, is also a pseudo-wurtzite cluster with a core similar to that larger In₃₇P₂₀ cluster but likely without the terminating cations, giving a best guess of Cd₂₁Se₂₀. In₂₆As₁₈ shares structural similarities with the InP clusters but is distinct in having an abundance of three coordinate pnictide ions at the surface, similar to what is seen for the structurally characterized pseudo-wurtzite CdSe clusters, including Cd₂₆Se₁₇. In the II-VI cluster universe, there are also well-characterized examples of zincblende cluster polymorphs with rigorously tetrahedral core symmetry - analogous clusters have yet to be definitively identified in the III-V family.

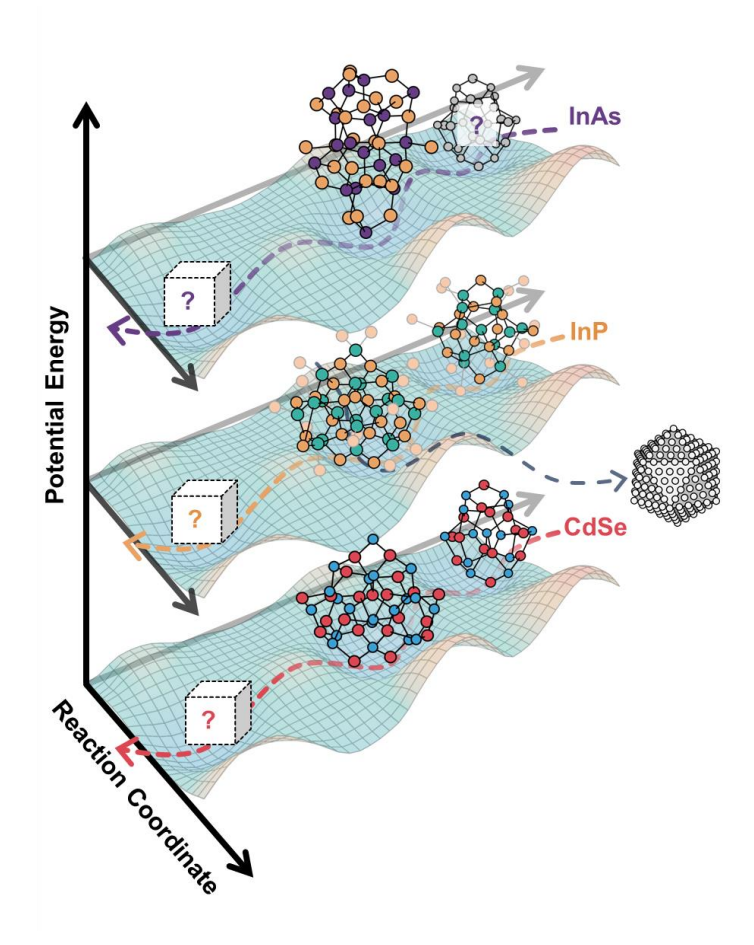


Figure 6: Illustration of energy landscapes of II-VI and III-V MSCs, highlighting their structural homologies, potential conversion pathways, and opportunities for new structure discoveries.

The possibility of uncovering other structural classes and new phases remains an exciting frontier. Our findings suggest that the known spectrum of nanocluster structures is just the tip of the iceberg, with immense potential for novel structures waiting to be discovered. This exploration is further complemented by the role of ligands in controlling structure and reactivity. Our research highlights how ligand chemistry can significantly influence the formation and transformation of MSCs, offering a tunable parameter for future material synthesis. Moreover, the role of MSCs as intermediates in the formation of larger nanocrystals cannot be overstated. It is quite possible that MSCs are universal to all compositions and phases, and it is only a matter of identifying conditions suited to their isolation. MSCs serve as crucial stepping stones, dictating the growth pathways and final properties of nanocrystals. This intermediary role underscores their significance in the broader context of materials science.

Looking ahead, the prospects of expanding structural and compositional diversity through cation exchange are particularly promising. Our work has laid the groundwork for this exploration, demonstrating the feasibility and potential of such transformations. This approach could unlock new avenues for material design, enabling the creation of nanomaterials with tailored properties for various applications.

Our research on II-VI and III-V MSCs provides valuable insights into the fundamental principles governing their structure and reactivity. The structural homologies, connections to bulk phases, and the role of ligands and cation exchange in controlling these properties offer exciting opportunities for developing novel nanomaterials. As we continue to explore these tiny yet complex structures, we open up new possibilities for advancing the field of nanotechnology.

Biographical Information

Hunter H. Ripberger received his B.S. in Chemistry from the University of North Carolina at Chapel Hill in 2016 and his Ph.D. from Princeton University in 2021. He is currently a postdoctoral scholar at the University of Washington in the laboratory of Brandi Cossairt. His research interests include the synthesis, characterization, and reactivity of II-VI magic-sized clusters.

Soren F. Sandeno received his B.A in Chemistry from Whitman College in 2021 and is a PhD student at the University of Washington. Soren's thesis work focuses on characterizing III-V cluster structure and reactivity.

Forrest W. Eagle received his B.S. in Chemistry with a Biochemistry option from Fort Lewis College in 2017 and his Ph.D. from the University of Washington in 2024. Forrest's thesis work focused on coinage metal cation exchange in InP quantum dots and clusters.

Hao A. Nguyen received his B.S. degree in Chemistry from Texas A&M University in 2020. He is pursuing his Ph.D. degree in Chemistry at the University of Washington under the supervision

of Brandi Cossairt. His research interests include developing inorganic shelling techniques for Cd-, In-, and Pb-based quantum dots and other emissive colloidal systems. Additionally, he aims to leverage machine-learning algorithms to aid in the synthesis of nanocrystals. His overarching research goal is to develop a stable, efficient, scalable, and highly emissive platform for quantum photonics applications.

Brandi M. Cossairt received her B.S. in Chemistry from the California Institute of Technology in 2006 and her Ph.D. from the Massachusetts Institute of Technology in 2010. She then trained as an NIH NRSA Postdoctoral Fellow at Columbia University before joining the Department of Chemistry at the University of Washington where she is currently the Lloyd E. and Florence M. West Endowed Professor. Her research group examines the nucleation, growth, surface chemistry, and reactivity of nanoscale materials to enable next-generation technologies in the diverse areas of displays, lighting, catalysis, quantum information, and hybrid matter.

Acknowledgments

We gratefully acknowledge support from the National Science Foundation CHE-2107237 for support of H.H.R. and S.F.S. (III-V and II-VI cluster synthesis and surface chemistry) and NSF DMR-2308979 for support of F.W.E. (cluster cation exchange and doping).

References

- (1) Jin, R.; Zeng, C.; Zhou, M.; Chen, Y. Atomically Precise Colloidal Metal Nanoclusters and Nanoparticles: Fundamentals and Opportunities. *Chem. Rev.* **2016**, *116* (18), 10346–10413. https://doi.org/10.1021/acs.chemrev.5b00703.
- (2) Qian, H.; Zhu, M.; Wu, Z.; Jin, R. Quantum Sized Gold Nanoclusters with Atomic Precision. *Acc. Chem. Res.* **2012**, *45* (9), 1470–1479. https://doi.org/10.1021/ar200331z.
- (3) Chakraborty, I.; Pradeep, T. Atomically Precise Clusters of Noble Metals: Emerging Link between Atoms and Nanoparticles. *Chem. Rev.* **2017**, *117* (12), 8208–8271. https://doi.org/10.1021/acs.chemrev.6b00769.
- (4) Yao, Q.; Chen, T.; Yuan, X.; Xie, J. Toward Total Synthesis of Thiolate-Protected Metal Nanoclusters. *Acc. Chem. Res.* **2018**, *51* (6), 1338–1348. https://doi.org/10.1021/acs.accounts.8b00065.
- (5) Walter, M.; Akola, J.; Lopez-Acevedo, O.; Jadzinsky, P. D.; Calero, G.; Ackerson, C. J.; Whetten, R. L.; Grönbeck, H.; Häkkinen, H. A Unified View of Ligand-Protected Gold Clusters as Superatom Complexes. *Proc. Natl. Acad. Sci.* **2008**, *105* (27), 9157–9162. https://doi.org/10.1073/pnas.0801001105.
- (6) Castleman, A. W. Jr.; Khanna, S. N. Clusters, Superatoms, and Building Blocks of New Materials. *J. Phys. Chem. C* **2009**, *113* (7), 2664–2675. https://doi.org/10.1021/jp806850h.
- (7) Luo, Z.; Castleman, A. W. Special and General Superatoms. *Acc. Chem. Res.* **2014**, *47* (10), 2931–2940. https://doi.org/10.1021/ar5001583.
- (8) Tang, Q.; Hu, G.; Fung, V.; Jiang, D. Insights into Interfaces, Stability, Electronic Properties, and Catalytic Activities of Atomically Precise Metal Nanoclusters from First Principles. *Acc. Chem. Res.* **2018**, *51* (11), 2793–2802. https://doi.org/10.1021/acs.accounts.8b00380.
- (9) Taylor, M. G.; Mpourmpakis, G. Thermodynamic Stability of Ligand-Protected Metal Nanoclusters. *Nat. Commun.* **2017**, *8* (1), 15988. https://doi.org/10.1038/ncomms15988.

- (10) Kasuya, A.; Sivamohan, R.; Barnakov, Y. A.; Dmitruk, I. M.; Nirasawa, T.; Romanyuk, V. R.; Kumar, V.; Mamykin, S. V.; Tohji, K.; Jeyadevan, B.; Shinoda, K.; Kudo, T.; Terasaki, O.; Liu, Z.; Belosludov, R. V.; Sundararajan, V.; Kawazoe, Y. Ultra-Stable Nanoparticles of CdSe Revealed from Mass Spectrometry. *Nat. Mater.* **2004**, *3* (2), 99–102. https://doi.org/10.1038/nmat1056.
- (11) Nguyen, K. A.; Day, P. N.; Pachter, R. Understanding Structural and Optical Properties of Nanoscale CdSe Magic-Size Quantum Dots: Insight from Computational Prediction. *J. Phys. Chem. C* **2010**, *114* (39), 16197–16209. https://doi.org/10.1021/jp103763d.
- (12) Nguyen, K. A.; Pachter, R.; Day, P. N. Computational Prediction of Structures and Optical Excitations for Nanoscale Ultrasmall ZnS and CdSe Clusters. *J. Chem. Theory Comput.* **2013**, *9* (8), 3581–3596. https://doi.org/10.1021/ct4001944.
- (13) Nguyen, K. A.; Pachter, R.; Day, P. N.; Su, H. Theoretical Analysis of Structures and Electronic Spectra in Molecular Cadmium Chalcogenide Clusters. *J. Chem. Phys.* **2015**, *142* (23), 234305. https://doi.org/10.1063/1.4922320.
- (14) Nguyen, K. A.; Pachter, R.; Jiang, J.; Day, P. N. Systematic Study of Structure, Stability, and Electronic Absorption of Tetrahedral CdSe Clusters with Carboxylate and Amine Ligands. *J. Phys. Chem. A* **2018**, *122* (33), 6704–6712. https://doi.org/10.1021/acs.jpca.8b02813.
- (15) Nguyen, K. A.; Pachter, R.; Day, P. N. Systematic Study of the Properties of CdS Clusters with Carboxylate Ligands Using a Deep Neural Network Potential Developed with Data from Density Functional Theory Calculations. *J. Phys. Chem. A* **2020**, *124* (50), 10472–10481. https://doi.org/10.1021/acs.jpca.0c06965.
- (16) Behrens, S.; Bettenhausen, M.; Deveson, A. C.; Eichhöfer, A.; Fenske, D.; Lohde, A.; Woggon, U. Synthesis and Structure of the Nanoclusters [Hg32Se14(SePh)36], [Cd32Se14(SePh)36-(PPh3)4],[P(Et)2(Ph)C4H8OSiMe3]5- [Cd18I17(PSiMe3)12], and [N(Et)3C4H8OSiMe3]5[Cd18I17(PSiMe3)12]. *Angew. Chem. Int. Ed. Engl.* 1996, *35* (19), 2215–2218. https://doi.org/10.1002/anie.199622151.
- (17) Eichhöfer, A. Thermal Properties of [M10Se4(SePh)12(PR3)4] (M = Zn, Cd, Hg)Cluster Molecules Synthesis and Structure of [Cd32Se14(SePh)36(L)4]; L = OPPh3, OC4H8. *Eur. J. Inorg. Chem.* **2005**, *2005* (7), 1245–1253. https://doi.org/10.1002/ejic.200400799.
- (18) Soloviev, V. N.; Eichhöfer, A.; Fenske, D.; Banin, U. Molecular Limit of a Bulk Semiconductor: Size Dependence of the "Band Gap" in CdSe Cluster Molecules. *J. Am. Chem. Soc.* **2000**, *122* (11), 2673–2674. https://doi.org/10.1021/ja9940367.
- (19) Soloviev, V. N.; Eichhöfer, A.; Fenske, D.; Banin, U. Size-Dependent Optical Spectroscopy of a Homologous Series of CdSe Cluster Molecules. *J. Am. Chem. Soc.* **2001**, *123* (10), 2354–2364. https://doi.org/10.1021/ja003598j.
- (20) Kudera, S.; Zanella, M.; Giannini, C.; Rizzo, A.; Li, Y.; Gigli, G.; Cingolani, R.; Ciccarella, G.; Spahl, W.; Parak, W. J.; Manna, L. Sequential Growth of Magic-Size CdSe Nanocrystals. *Adv. Mater.* **2007**, *19* (4), 548–552. https://doi.org/10.1002/adma.200601015.
- (21) Beecher, A. N.; Yang, X.; Palmer, J. H.; LaGrassa, A. L.; Juhas, P.; Billinge, S. J. L.; Owen, J. S. Atomic Structures and Gram Scale Synthesis of Three Tetrahedral Quantum Dots. *J. Am. Chem. Soc.* **2014**, *136* (30), 10645–10653. https://doi.org/10.1021/ja503590h.
- (22) Mule, A. S.; Mazzotti, S.; Rossinelli, A. A.; Aellen, M.; Prins, P. T.; Van Der Bok, J. C.; Solari, S. F.; Glauser, Y. M.; Kumar, P. V.; Riedinger, A.; Norris, D. J. Unraveling the Growth Mechanism of Magic-Sized Semiconductor Nanocrystals. *J. Am. Chem. Soc.* **2021**, *143* (4), 2037–2048. https://doi.org/10.1021/jacs.0c12185.

- (23) Liu, Y.-H.; Wang, F.; Wang, Y.; Gibbons, P. C.; Buhro, W. E. Lamellar Assembly of Cadmium Selenide Nanoclusters into Quantum Belts. *J. Am. Chem. Soc.* **2011**, *133* (42), 17005–17013. https://doi.org/10.1021/ja206776g.
- (24) Wang, Y.; Zhang, Y.; Wang, F.; Giblin, D. E.; Hoy, J.; Rohrs, H. W.; Loomis, R. A.; Buhro, W. E. The Magic-Size Nanocluster (CdSe)34 as a Low-Temperature Nucleant for Cadmium Selenide Nanocrystals; Room-Temperature Growth of Crystalline Quantum Platelets. *Chem. Mater.* **2014**, *26* (7), 2233–2243. https://doi.org/10.1021/cm404068e.
- (25) Yu, J. H.; Liu, X.; Kweon, K. E.; Joo, J.; Park, J.; Ko, K.-T.; Lee, D. W.; Shen, S.; Tivakornsasithorn, K.; Son, J. S.; Park, J.-H.; Kim, Y.-W.; Hwang, G. S.; Dobrowolska, M.; Furdyna, J. K.; Hyeon, T. Giant Zeeman Splitting in Nucleation-Controlled Doped CdSe:Mn2+ Quantum Nanoribbons. *Nat. Mater.* **2010**, *9* (1), 47–53. https://doi.org/10.1038/nmat2572.
- (26) Joo, J.; Son, J. S.; Kwon, S. G.; Yu, J. H.; Hyeon, T. Low-Temperature Solution-Phase Synthesis of Quantum Well Structured CdSe Nanoribbons. *J. Am. Chem. Soc.* **2006**, *128* (17), 5632–5633. https://doi.org/10.1021/ja0601686.
- (27) Bootharaju, M. S.; Baek, W.; Deng, G.; Singh, K.; Voznyy, O.; Zheng, N.; Hyeon, T. Structure of a Subnanometer-Sized Semiconductor Cd14Se13 Cluster. *Chem* **2022**, *8* (11), 2978–2989. https://doi.org/10.1016/j.chempr.2022.06.025.
- (28) Sandeno, S. F.; Schnitzenbaumer, K. J.; Krajewski, S. M.; Beck, R. A.; Ladd, D. M.; Levine, K. R.; Dayton, D.; Toney, M. F.; Kaminsky, W.; Li, X.; Cossairt, B. M. Ligand Steric Profile Tunes the Reactivity of Indium Phosphide Clusters. *J. Am. Chem. Soc.* **2024**, *146* (5), 3102–3113. https://doi.org/10.1021/jacs.3c10203.
- (29) Gary, D. C.; Flowers, S. E.; Kaminsky, W.; Petrone, A.; Li, X.; Cossairt, B. M. Single-Crystal and Electronic Structure of a 1.3 Nm Indium Phosphide Nanocluster. *J. Am. Chem. Soc.* **2016**, *138* (5), 1510–1513. https://doi.org/10.1021/jacs.5b13214.
- (30) Bowers II, M. J.; McBride, J. R.; Garrett, M. D.; Sammons, J. A.; Dukes III, A. D.; Schreuder, M. A.; Watt, T. L.; Lupini, A. R.; Pennycook, S. J.; Rosenthal, S. J. Structure and Ultrafast Dynamics of White-Light-Emitting CdSe Nanocrystals. *J. Am. Chem. Soc.* **2009**, *131* (16), 5730–5731. https://doi.org/10.1021/ja900529h.
- (31) Dolai, S.; Nimmala, P. R.; Mandal, M.; Muhoberac, B. B.; Dria, K.; Dass, A.; Sardar, R. Isolation of Bright Blue Light-Emitting CdSe Nanocrystals with 6.5 kDa Core in Gram Scale: High Photoluminescence Efficiency Controlled by Surface Ligand Chemistry. *Chem. Mater.* **2014**, *26* (2), 1278–1285. https://doi.org/10.1021/cm403950f.
- (32) Cossairt, B. M.; Owen, J. S. CdSe Clusters: At the Interface of Small Molecules and Quantum Dots. *Chem. Mater.* **2011**, *23* (12), 3114–3119. https://doi.org/10.1021/cm2008686.
- (33) Ripberger, H. H.; Schnitzenbaumer, K. J.; Nguyen, L. K.; Ladd, D. M.; Levine, K. R.; Dayton, D. G.; Toney, M. F.; Cossairt, B. M. Navigating the Potential Energy Surface of CdSe Magic-Sized Clusters: Synthesis and Interconversion of Atomically Precise Nanocrystal Polymorphs. *J. Am. Chem. Soc.* 2023, 145 (50), 27480–27492. https://doi.org/10.1021/jacs.3c08897.
- (34) Xie, R.; Li, Z.; Peng, X. Nucleation Kinetics vs Chemical Kinetics in the Initial Formation of Semiconductor Nanocrystals. *J. Am. Chem. Soc.* **2009**, *131* (42), 15457–15466. https://doi.org/10.1021/ja9063102.

- (35) Gary, D. C.; Terban, M. W.; Billinge, S. J. L.; Cossairt, B. M. Two-Step Nucleation and Growth of InP Quantum Dots via Magic-Sized Cluster Intermediates. *Chem. Mater.* **2015**, *27* (4), 1432–1441. https://doi.org/10.1021/acs.chemmater.5b00286.
- (36) Friedfeld, M. R.; Johnson, D. A.; Cossairt, B. M. Conversion of InP Clusters to Quantum Dots. *Inorg. Chem.* **2019**, *58* (1), 803–810. https://doi.org/10.1021/acs.inorgchem.8b02945.
- (37) Li, Q.; Luo, T.-Y.; Zhou, M.; Abroshan, H.; Huang, J.; Kim, H. J.; Rosi, N. L.; Shao, Z.; Jin, R. Silicon Nanoparticles with Surface Nitrogen: 90% Quantum Yield with Narrow Luminescence Bandwidth and the Ligand Structure Based Energy Law. *ACS Nano* **2016**, *10* (9), 8385–8393. https://doi.org/10.1021/acsnano.6b03113.
- (38) Leger, J. D.; Friedfeld, M. R.; Beck, R. A.; Gaynor, J. D.; Petrone, A.; Li, X.; Cossairt, B. M.; Khalil, M. Carboxylate Anchors Act as Exciton Reporters in 1.3 Nm Indium Phosphide Nanoclusters. *J. Phys. Chem. Lett.* 2019, 10 (8), 1833–1839. https://doi.org/10.1021/acs.jpclett.9b00602.
- (39) Ritchhart, A.; Cossairt, B. M. Quantifying Ligand Exchange on InP Using an Atomically Precise Cluster Platform. *Inorg. Chem.* **2019**, *58* (4), 2840–2847. https://doi.org/10.1021/acs.inorgchem.8b03524.
- (40) Stein, J. L.; Steimle, M. I.; Terban, M. W.; Petrone, A.; Billinge, S. J. L.; Li, X.; Cossairt, B. M. Cation Exchange Induced Transformation of InP Magic-Sized Clusters. *Chem. Mater.* 2017, 29 (18), 7984–7992. https://doi.org/10.1021/acs.chemmater.7b03075.
- (41) Eagle, F. W.; Harvey, S.; Larson, H.; Abbott, A.; Ladd, D. M.; Levine, K. R.; Toney, M. F.; Gamelin, D. R.; Cossairt, B. M. Leveraging Cation Exchange in InP Magic-Sized Clusters To Access Coinage Metal Phosphide Nanocrystals. *Chem. Mater.* **2024**, *36* (6), 2888–2897. https://doi.org/10.1021/acs.chemmater.3c03258.
- (42) Ritchhart, A.; Cossairt, B. M. Templated Growth of InP Nanocrystals with a Polytwistane Structure. *Angew. Chem. Int. Ed.* **2018**, *57* (7), 1908–1912. https://doi.org/10.1002/anie.201711539.
- (43) Marion, D. An Introduction to Biological NMR Spectroscopy. *Mol. Cell. Proteomics MCP* **2013**, *12* (11), 3006–3025. https://doi.org/10.1074/mcp.O113.030239.
- (44) Xie, R.; Peng, X. Synthetic Scheme for High-Quality InAs Nanocrystals Based on Self-Focusing and One-Pot Synthesis of InAs-Based Core—Shell Nanocrystals. *Angew. Chem. Int. Ed.* **2008**, *47* (40), 7677–7680. https://doi.org/10.1002/anie.200802867.
- (45) Li, Y.; Hou, X.; Shen, Y.; Dai, N.; Peng, X. Tuning the Reactivity of Indium Alkanoates by Tertiary Organophosphines for the Synthesis of Indium-Based Quantum Dots. *Chem. Mater.* **2021**, *33* (23), 9348–9356. https://doi.org/10.1021/acs.chemmater.1c03219.
- (46) Harris, D. K.; Bawendi, M. G. Improved Precursor Chemistry for the Synthesis of III–V Quantum Dots. J. Am. Chem. Soc. 2012, 134 (50), 20211–20213. https://doi.org/10.1021/ja309863n.
- (47) Franke, D.; Harris, D. K.; Xie, L.; Jensen, K. F.; Bawendi, M. G. The Unexpected Influence of Precursor Conversion Rate in the Synthesis of III–V Quantum Dots. *Angew. Chem. Int. Ed.* **2015**, *54* (48), 14299–14303. https://doi.org/10.1002/anie.201505972.
- (48) Sandeno, S. F.; Krajewski, S. M.; Beck, R. A.; Kaminsky, W.; Li, X.; Cossairt, B. M. Synthesis and Single Crystal X-Ray Diffraction Structure of an Indium Arsenide Nanocluster. *ACS Cent. Sci.* **2024**, *10* (3), 744–751. https://doi.org/10.1021/acscentsci.3c01451.

- (49) Ma, F.; Abboud, K. A.; Zeng, C. Precision Synthesis of a CdSe Semiconductor Nanocluster via Cation Exchange. *Nat. Synth.* 2023, 2 (10), 949–959. https://doi.org/10.1038/s44160-023-00330-6.
- (50) Peng, Z. A.; Peng, X. Nearly Monodisperse and Shape-Controlled CdSe Nanocrystals via Alternative Routes: Nucleation and Growth. *J. Am. Chem. Soc.* **2002**, *124* (13), 3343–3353. https://doi.org/10.1021/ja0173167.
- (51) Jiang, Z.-J.; Kelley, D. F. Role of Magic-Sized Clusters in the Synthesis of CdSe Nanorods. *ACS Nano* **2010**, *4* (3), 1561–1572. https://doi.org/10.1021/nn100076f.
- (52) Williamson, C. B.; Nevers, D. R.; Nelson, A.; Hadar, I.; Banin, U.; Hanrath, T.; Robinson, R. D. Chemically Reversible Isomerization of Inorganic Clusters. *Science* **2019**, *363* (6428), 731–735. https://doi.org/10.1126/science.aau9464.
- (53) He, L.; Luan, C.; Rowell, N.; Zhang, M.; Chen, X.; Yu, K. Transformations Among Colloidal Semiconductor Magic-Size Clusters. *Acc. Chem. Res.* **2021**, *54* (4), 776–786. https://doi.org/10.1021/acs.accounts.0c00702.
- (54) Zhang, B.; Zhu, T.; Ou, M.; Rowell, N.; Fan, H.; Han, J.; Tan, L.; Dove, M. T.; Ren, Y.; Zuo, X.; Han, S.; Zeng, J.; Yu, K. Thermally-Induced Reversible Structural Isomerization in Colloidal Semiconductor CdS Magic-Size Clusters. *Nat. Commun.* **2018**, *9* (1), 2499. https://doi.org/10.1038/s41467-018-04842-0.
- (55) Zhu, D.; Hui, J.; Rowell, N.; Liu, Y.; Chen, Q. Y.; Steegemans, T.; Fan, H.; Zhang, M.; Yu, K. Interpreting the Ultraviolet Absorption in the Spectrum of 415 Nm-Bandgap CdSe Magic-Size Clusters. *J. Phys. Chem. Lett.* 2018, 9 (11), 2818–2824. https://doi.org/10.1021/acs.jpclett.8b01109.
- (56) Gao, D.; Hao, X.; Rowell, N.; Kreouzis, T.; Lockwood, D. J.; Han, S.; Fan, H.; Zhang, H.; Zhang, C.; Jiang, Y.; Zeng, J.; Zhang, M.; Yu, K. Formation of Colloidal Alloy Semiconductor CdTeSe Magic-Size Clusters at Room Temperature. *Nat. Commun.* 2019, 10 (1), 1674. https://doi.org/10.1038/s41467-019-09705-w.
- (57) He, L.; Luan, C.; Liu, S.; Chen, M.; Rowell, N.; Wang, Z.; Li, Y.; Zhang, C.; Lu, J.; Zhang, M.; Liang, B.; Yu, K. Transformations of Magic-Size Clusters via Precursor Compound Cation Exchange at Room Temperature. *J. Am. Chem. Soc.* **2022**, *144* (41), 19060–19069. https://doi.org/10.1021/jacs.2c07972.
- (58) Zhao, Q.; Kulik, H. J. Electronic Structure Origins of Surface-Dependent Growth in III– V Quantum Dots. *Chem. Mater.* 2018, 30 (20), 7154–7165. https://doi.org/10.1021/acs.chemmater.8b03125.
- (59) Nevers, D. R.; Williamson, C. B.; Hanrath, T.; Robinson, R. D. Surface Chemistry of Cadmium Sulfide Magic-Sized Clusters: A Window into Ligand-Nanoparticle Interactions. *Chem. Commun.* **2017**, *53* (19), 2866–2869. https://doi.org/10.1039/C6CC09549F.
- (60) White, S. L.; Banerjee, P.; Chakraborty, I.; Jain, P. K. Ion Exchange Transformation of Magic-Sized Clusters. *Chem. Mater.* 2016, 28 (22), 8391–8398. https://doi.org/10.1021/acs.chemmater.6b03882.
- (61) Muckel, F.; Yang, J.; Lorenz, S.; Baek, W.; Chang, H.; Hyeon, T.; Bacher, G.; Fainblat, R. Digital Doping in Magic-Sized CdSe Clusters. ACS Nano 2016, 10 (7), 7135–7141. https://doi.org/10.1021/acsnano.6b03348.
- (62) Yang, J.; Fainblat, R.; Kwon, S. G.; Muckel, F.; Yu, J. H.; Terlinden, H.; Kim, B. H.; Iavarone, D.; Choi, M. K.; Kim, I. Y.; Park, I.; Hong, H.-K.; Lee, J.; Son, J. S.; Lee, Z.; Kang, K.; Hwang, S.-J.; Bacher, G.; Hyeon, T. Route to the Smallest Doped Semiconductor:

- Mn2+-Doped (CdSe)13 Clusters. *J. Am. Chem. Soc.* **2015**, *137* (40), 12776–12779. https://doi.org/10.1021/jacs.5b07888.
- (63) Yang, J.; Muckel, F.; Choi, B. K.; Lorenz, S.; Kim, I. Y.; Ackermann, J.; Chang, H.; Czerney, T.; Kale, V. S.; Hwang, S.-J.; Bacher, G.; Hyeon, T. Co2+-Doping of Magic-Sized CdSe Clusters: Structural Insights via Ligand Field Transitions. *Nano Lett.* **2018**, *18* (11), 7350–7357. https://doi.org/10.1021/acs.nanolett.8b03627.
- (64) Pittala, S.; Mortelliti, M. J.; Kato, F.; Kittilstved, K. R. Substitution of Co2+ Ions into CdS-Based Molecular Clusters. *Chem. Commun.* **2015**, *51* (96), 17096–17099. https://doi.org/10.1039/C5CC06138E.
- (65) Pittala, S.; Kittilstved, K. R. Cation Exchange in Small ZnS and CdS Molecular Analogues. *Inorg. Chem.* **2015**, *54* (12), 5757–5767. https://doi.org/10.1021/acs.inorgchem.5b00421.
- (66) Kato, F.; Kittilstved, K. R. Site-Specific Doping of Mn2+ in a CdS-Based Molecular Cluster. *Chem. Mater.* 2018, 30 (14), 4720–4727. https://doi.org/10.1021/acs.chemmater.8b01482.
- (67) Kong, X.; Deng, Y.; Zou, Y.; Ge, J.; Wang, Y. Anion Exchange in Semiconductor Magic-Size Clusters. *J. Am. Chem. Soc.* **2024**, *146* (8), 5445–5454. https://doi.org/10.1021/jacs.3c12853.
- (68) Dumett Torres, D.; Jain, P. K. Ab Initio Investigation of Cooperativity in Ion Exchange. *J. Phys. Chem. C* **2020**, *124* (46), 25615–25620. https://doi.org/10.1021/acs.jpcc.0c08197.
- (69) Routzahn, A. L.; Jain, P. K. Single-Nanocrystal Reaction Trajectories Reveal Sharp Cooperative Transitions. *Nano Lett.* **2014**, *14* (2), 987–992. https://doi.org/10.1021/nl4044289.
- (70) Yao, Y.; Lynch, R.; Robinson, R. D. Mass Spectroscopy Study of the Intermediate Magic-Size Cluster Species during Cooperative Cation Exchange. *J. Chem. Phys.* **2023**, *159* (1), 014704. https://doi.org/10.1063/5.0151904.
- (71) Friedfeld, M. R.; Stein, J. L.; Johnson, D. A.; Park, N.; Henry, N. A.; Enright, M. J.; Mocatta, D.; Cossairt, B. M. Effects of Zn2+ and Ga3+ Doping on the Quantum Yield of Cluster-Derived InP Quantum Dots. *J. Chem. Phys.* 2019, 151 (19), 194702. https://doi.org/10.1063/1.5126971.
- (72) Hughes, K. E.; Stein, J. L.; Friedfeld, M. R.; Cossairt, B. M.; Gamelin, D. R. Effects of Surface Chemistry on the Photophysics of Colloidal InP Nanocrystals. *ACS Nano* **2019**, *13* (12), 14198–14207. https://doi.org/10.1021/acsnano.9b07027.
- (73) Gary, D. C.; Petrone, A.; Li, X.; Cossairt, B. M. Investigating the Role of Amine in InP Nanocrystal Synthesis: Destabilizing Cluster Intermediates by Z-Type Ligand Displacement. *Chem. Commun.* **2016**, *53* (1), 161–164. https://doi.org/10.1039/C6CC07952K.
- (74) Taylor, M. G.; Kulik, H. J. Mapping the Origins of Surface- and Chemistry-Dependent Doping Trends in III–V Quantum Dots with Density Functional Theory. *Chem. Mater.* **2021**, 33 (17), 7113–7123. https://doi.org/10.1021/acs.chemmater.1c02556.
- (75) Shim, D.; Kang, J. Enhanced Reactivity of Magic-Sized Inorganic Clusters by Engineering the Surface Ligand Networks. *Chem. Mater.* **2023**, *35* (2), 700–708. https://doi.org/10.1021/acs.chemmater.2c03394.